

TRAILING EDGE FLOW CONTROL FOR THE MITIGATION OF DYNAMIC STALL EFFECTS

Gregory L. Davisⁱ, Daniel Fesztyⁱⁱ, and Fred Nitzscheⁱⁱⁱ
Mechanical and Aerospace Engineering
Carleton University
Ottawa, ON, K1S 5B6, Canada

ABSTRACT

The use of an actively controlled flap for the reduction of dynamic stall induced vibration is demonstrated via CFD. Two separate flap actuations are considered. In the first instance, a moderate advance ratio dynamic stall case is examined by using a 3D Aeroelastic code, GAST, which couples a vortex particle method, and dynamics equations for a beam model. This case employs a downward flap deflection to reduce the portion of the rotor disk area over which dynamic stall is encountered. The second approach targets dynamic stall occurring in high advance ratio forward flight configurations. 2D RANS simulations were performed. In this case, an upward flap deflection is employed in order to control the strength of the trailing edge vortex. In both cases the flap served to reduce the amplitudes of vertical blade reaction forces, blade torsional moment and negative aerodynamic damping, indicating a net reduction in the vibration experienced by the rotors.

Introduction

Noise and vibration affect helicopters operating within their normal flight envelope. Noise presents a disturbance to people on the ground and vibrations reduce passenger comfort, controllability, and the operational life of a helicopter. Furthermore, vibrations can achieve such magnitude that they present a danger of catastrophic failure of the rotor blades. The source of noise is acoustic pressure generated by the rotor blades. The most offensive source of acoustic pressure is blade-vortex interaction (BVI), which is the interaction of the helical tip vortices with the rotor blades.

Vibrations are induced at several stages of flight, with shock induced vibrations occurring on the advancing blades and dynamic stall induced vibrations, including stall flutter, on the retreating ones. Additionally, inertial and structural loads transmitted through the blades into the rotor hub contribute to vibrations. There exists a conundrum in respect to the elimination of vibration and noise. Research by Friedmann [1] and Klöppel [2] has demonstrated that the reduction of one of these results in an increase of the other.

There are several approaches for reducing noise or vibration. Friedmann [3], Fulton [4] and Klöppel [2] employ one or more actively controlled trailing edge flaps (ACF). NASA, the US ARMY and MIT have

proposed the use of active twist rotor (ATR) [5]. Research on individual blade control (IBC) has been conducted for many years. There is also research into an actively controlled leading edge flap, and into higher harmonic control (HHC). This paper will focus on the actively controlled trailing edge flap, with the intent of employing it in the Smart Hybrid Active Rotor Control System (SHARCS) project, as described by Nitzsche et al [6].

The trailing edge flap was selected over the other options based on the ease of implementation and small actuation forces in comparison to leading edge devices. Existing technology, in terms of actuators and control systems, is at a level that can support the needs of a small scale flap as proposed in the SHARCS project. The structural constraints limit the flap to approximately 20% relative chord.

Research on the use of ACF concepts to date includes CFD simulations conducted by Friedmann [3], and Barakos et al [7]. Wind tunnel tests have been conducted by Chopra [8] and whirl tower tests by Boeing Mesa [8] and Eurocopter [2], with the first flight testing scheduled for the very near future.

Computational Fluid Dynamics will remain an important part of ACF research, even as experimental work begins. The results from

ⁱ Research Assistant.

ⁱⁱ Assistant Professor.

ⁱⁱⁱ Professor.

experiments and the semi-empirical results obtained to date, for 2P (2 per rev), 3P, or 4P actuations of the flap have not revealed a complete picture of the physical flow mechanism. CFD results can enable the detailed examination of the flow field so that the flap actuation strategy can be optimized, and can appear useful in complementing wind tunnel programmes in order to make them more efficient. It could also be used as a design tool, enabling the exploration of new actuation strategies, and flap designs.

The purpose of the present paper is to demonstrate the feasibility of ACF for the reduction of vibration on rotors via CFD. In particular, the vibrations due to dynamic stall will be targeted with the aim of avoiding or mitigating the effects of this phenomenon. Two strategies will be considered. At moderate advance ratios reduction of dynamic stall was attempted by producing the required amount of lift on the retreating blades via deflecting the flap downwards. At high advance ratios, on the other hand, when dynamic stall can no longer be avoided, the flap will be used to mitigate the effects of dynamic stall by deflecting it upwards.

The paper is divided into two parts. In the first part a 3D CFD simulation of a rotor with an ACF in forward flight will be performed. This should allow the simulation of the flap at moderate advance ratios for avoiding dynamic stall. The method used is a 3D Vortex Particle method with the ONERA dynamic stall model which, however, only models the effects of dynamic stall, but does not simulate the phenomenon itself. Therefore, for the cases when dynamic stall needs to be simulated, a 2D RANS solver will be used to demonstrate the feasibility of the other ACF strategy of mitigating the effects of dynamic stall.

Test Case

The two test cases are representative of the aerodynamic conditions experienced by a helicopter in forward flight. The 3D test case resembles a moderate advance ratio forward flight configuration with dynamic stall appearing on the retreating rotor blades. The geometry is based on the SHARCS rotor [6], and summarized in table 1.

Description	Value
Rotor Radius (R)	1m
Chord Length (c)	0.0563 m
Number of Blades	4
Type (N)	Hingeless
Airfoil Section	NACA 23012 (modified)
Twist	-4°
RPM	1340 min ⁻¹
Advance Ratio (μ)	0.35
Freestream Density (ρ)	1.225 kg/m ³

Table 1: 3D test case of a helicopter in forward flight

The second test case involves the simulation of a 2D airfoil based on the dynamic stall experimental data of the University of Glasgow [9]. The baseline dynamic stall test case is presented in Table 2.

Description	Value
Mach Number (M)	0.117
Reynolds Number (Re)	1,463,296
Reduced Frequency (k)	0.173
Airfoil Section	NACA 0012
Airfoil Motion	$\alpha(t) = 15^\circ + 10^\circ \sin(2kt)$

Table 2: 2D dynamic stall test case

The flap is introduced in the computational models in the following manner. For the 3D case, a single flap of 15% relative chord length is used. The flap is located spanwise from 70% to 90% of the radius. The 2D case tests three flap sizes, 10, 15 and 20% relative chord length. The flap size and location was selected primarily on the basis of the expected manufacturing constraints of the SHARCS rotor. The maximum flap deflection studied in the 3D case was 10°, and in the 2D case was 20° based on the constraints of the panel method, and the expected limitations of the actuators, respectively.

Flap Actuation Strategy

As indicated earlier, this paper studies two different uses of an actively controlled trailing edge flap. The flap itself remains the same; it is only the actuation that differs based on the flight regime. In both cases, the aim is to reduce vibration due to dynamic stall.

At low advance ratios, the flap will be deflected downward on the retreating blade, in order to generate the same lift as on the advancing blade, but at lower angle of attack, without entering dynamic stall. By this, dynamic stall is expected to be avoided since the stall angle of attack may not be exceeded.

This strategy can be successful only up to a certain forward flight speed. Beyond that, even with the downward flap deflection, the retreating blades would be forced to enter dynamic stall in order to maintain level flight. This can lead to stall flutter, and excessive vibrations in the pitch link loads, which eventually limit the maximum forward flight speed of the rotorcraft. Hence, it is suggested that for the cases when dynamic stall cannot be avoided (high advance ratios), the flap be deflected upwards to alleviate the negative effects of dynamic stall. More specifically, negative pitching moments and the associated negative aerodynamic damping will be aimed to be reduced [10].

3D Simulations

3D simulation of a rotorcraft in equilibrium forward flight was conducted in order to determine the effect of an actively controlled trailing edge flap on dynamic stall caused vibrations. Flight conditions were selected such that the uncontrolled (no flap actuation) test case was in the dynamic stall regime, with the controlled (flapped) case allowing the rotor blades to remain free of the dynamic stall regime.

Geometry Generation

A major advantage of a vortex particle method is that it does not require a grid, i.e. the computational domain need not be discretized into a mesh, yielding significant savings in the computational costs. However, solid surfaces have to be generated and discretized into panels. The flap is modeled simply by directly altering the position of the relevant nodes while the panels are being solved for each flow condition.

The 3D simulations use a four bladed SHARCS hingeless rotor. Each of the blades is identically composed of 98 panels, with a total of 120 nodes per blade. The spanwise distribution of the nodes is geometric, providing the highest panel density at the tip.

Numerical Method

The 3D modeling of a helicopter in forward flight was done using the GAST code, which was developed at the National Technical University of Athens [11]. It couples aerodynamic, structural, and acoustic components, of which a brief description is provided in the following.

Aerodynamic Component The aerodynamic component of GAST, is an unsteady code that employs a panel method for the solution of solid surfaces, and a vortex-particle representation of the wake, with viscosity and compressibility corrections for improved fidelity. The Helmholtz decomposition provides the basis for the code, separating the flow into irrotational and rotational parts, corresponding to surfaces and their wakes, respectively. It is defined as $\vec{u}(\vec{x}, t)$, $\vec{x} \in D$, $t \geq 0$, where \vec{x} is position, t is time and D the computational domain. The Helmholtz decomposition will be:

$$\vec{u}(\vec{x}, t) = \vec{u}_{ext}(\vec{x}, t) + \vec{u}_{solid}(\vec{x}, t) + \vec{u}_{near-wake}(\vec{x}, t) + \vec{u}_{far-wake}(\vec{x}, t) \quad (1)$$

Here \vec{u}_{ext} is analogous to V_∞ and is user defined.

The term \vec{u}_{solid} is velocity field resulting from the influence of solid bodies, representing the irrotational part of the decomposition. The term $\vec{u}_{near-wake}$ represents the wake effects in D near the solid. The term $\vec{u}_{far-wake}$ represents the wake effects in D far from the solid. The aerodynamic component of GAST uses a panel method to determine \vec{u}_{solid} , and $\vec{u}_{near-wake}$, while the Biot-Savart law is used to obtain $\vec{u}_{far-wake}$ according to:

$$\vec{u}_{far-wake}(\vec{x}, t) = \int_{D_\omega(t)} \frac{\vec{\omega}(\vec{x}_o, t) \times (\vec{x} - \vec{x}_o)}{4\pi|\vec{x} - \vec{x}_o|^3} dD \quad (2)$$

GAST uses the ONERA dynamic stall model to combine the overall calculated flow characteristics by 2D tabular profile data. This provides good results for both separated and attached flow conditions [12].

Structural Component The structural component of GAST is a linear elastic beam model combined with linearized multi-body dynamics. The beam equations are constructed in a Cartesian coordinate system with the y-axis denoting the undeformed elastic axis, which is analogous to the span of a rotor blade. The beam is subjected to flapping, lead-lag bending, radial flexion, and torsion. Detailed derivation of the structural and dynamic code is available in Ref. 11.

Acoustic Component The acoustic model is based on the Ffowcs Williams and Hastings (FW-H) equations. GAST uses the Farassat 1A approximation which enables the calculation of the thickness noise and momentum noise, while sacrificing the quadrupole noise, which is typically considered to be negligible.

Validation of the numerical method

Extensive validation of the GAST code was undertaken by Opoku [13], with comparisons to the HELINOISE experiment [9].

Flap Actuation Timing

The flap is actuated downward so that the angle of attack needed to maintain lift can be reduced. As such, the peak flap deflection was timed to occur at the peak lift which occurs at $\phi=270^\circ$ (azimuth angle). The actuation is sinusoidal over one quarter of the revolution, as shown in Fig. 1.

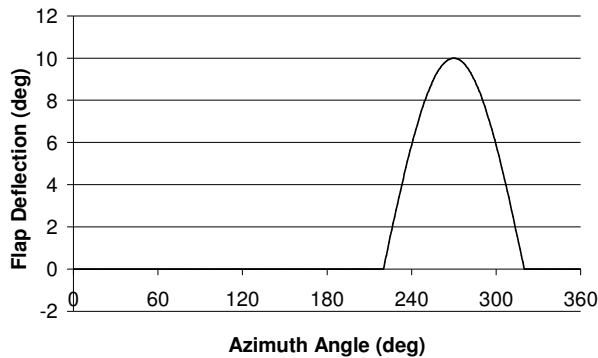


Figure 1: Flap actuation with respect to Azimuth (ϕ).

Results

The results were compared between the uncontrolled case and the controlled case for the 3D simulations. Of interest were the internal structural reactions at the blade root in the vertical direction, and the blade torsional moment about the feathering axis. These correlate to the vertical loads experienced at the blade root and the pitch link loads, respectively.

The duration of the calculations is dependant on the trim conditions of the rotor. The uncontrolled case converged after 103 revolutions. The final trim values from that case were then used as a basis for the controlled case, which converged after 21 revolutions. The non-dimensional time displayed in Figs. 2 to 5 are normalized to the first converged step for both cases, with the case of least computational error centered at $t = 0.29$.

It was first necessary to ensure that the lift created for a revolution of the blade remained the same for the uncontrolled and controlled cases. Variation in the overall lift would correlate to a change in the equilibrium forward flight state, which would invalidate any comparison of the internal loads and moments. A comparison of blade lift coefficient at 0.75R is shown in Fig. 2. Analysis of the lift generated by the rotor blades reveals a cumulative error of 1.44% for the two cycles shown, which appears to be an acceptable level of agreement.

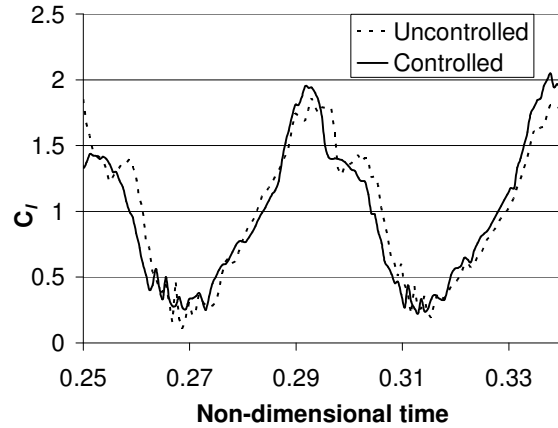


Figure 2: Blade lift coefficient at 0.75R.

The maximum angle of attack attained at 0.75R by the uncontrolled case was 16.2° . Since the static stall angle for the NACA 23012 airfoil is 14.6° at the operating Reynolds number, dynamic stall clearly occurs, Fig. 3. When the flap is employed, the maximum angle of attack is reduced to 15° , as expected. Although this is still beyond the critical angle of attack, it clearly shows that the ACF concept can delay dynamic stall and reduce the stalled flow area of the rotor disk.

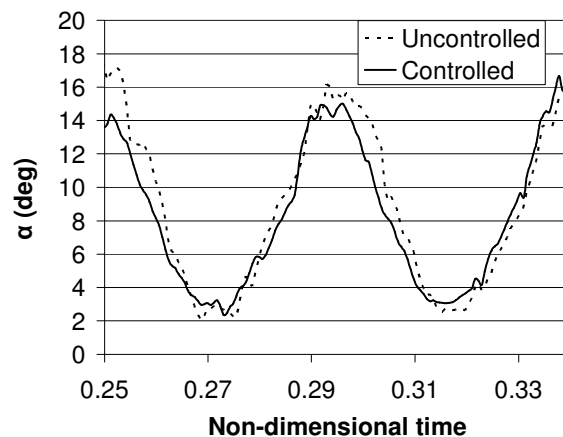


Figure 3: α with respect to non-dimensional time.

Fig. 4 shows the comparison of the internal structural reactions, F_z . The average decrease in the amplitude of vibration over the analyzed time period was 23% due to the flap actuation, when comparing the peak amplitudes for the converged results.

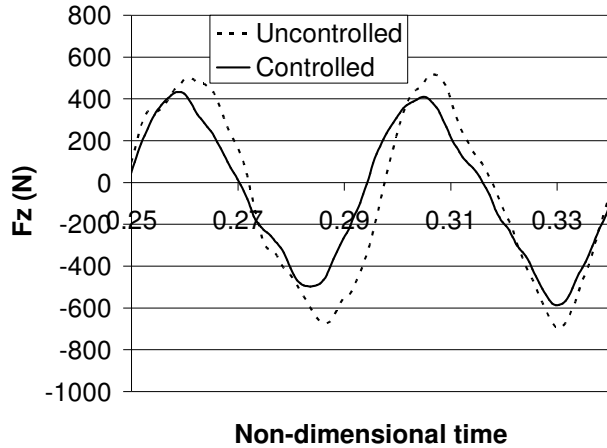


Figure 4: F_z with respect to non-dimensional time.

Finally, a comparison of the integrated torsional moments at the blade root is shown in Fig. 5. It can be seen that the reduction of these loads is much more dramatic than that of the vertical loads, with the peak moments reduced by as much as 44%. Since the torsional moments are transferred to the rotor hub via the pitch link rods, it can be concluded that a major benefit of the ACF concept in the moderate advance ratio case is the reduction of the vibratory levels in the pitch link loads.

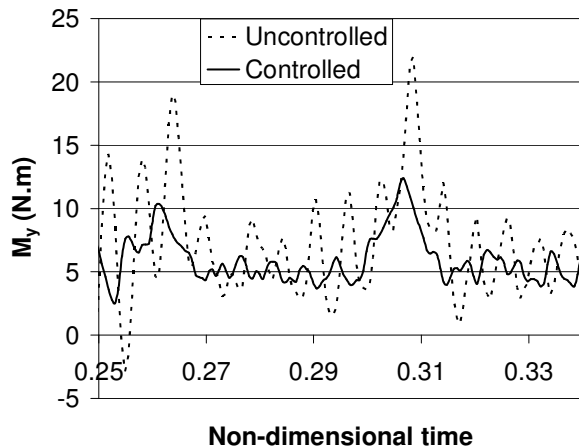


Figure 5: M_y with respect to non-dimensional time.

2D Simulations

The CMB code was used for simulating upward flap deflection cases for mitigating the effects of dynamic stall. This is a structured multi-block RANS solver based on PMB, a code originally developed at the University of Glasgow [14].

Mesh Generation

A structured multi-block C-topology mesh consisting of 95,000 nodes in 10 blocks was generated for the NACA 0012 airfoil (Fig. 6). The y^+ value at the wall was 8 and the distance from the surface to the outer boundary of the computational domain was 10 chord lengths.

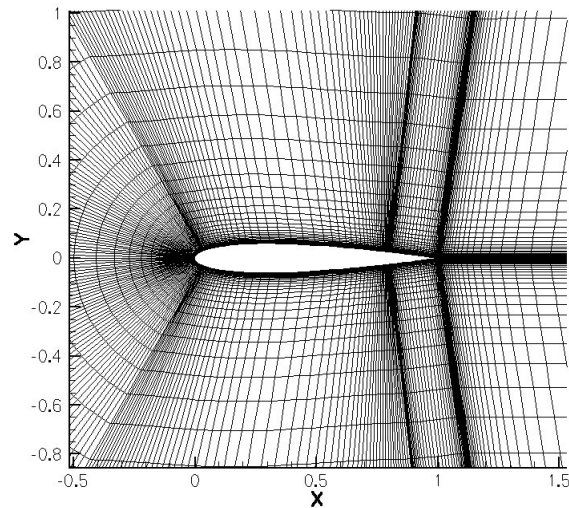


Figure 6: Computational mesh for the NACA 0012 airfoil.

The blocking was arranged in accordance with the location of the trailing edge flap. The blocks joining the freestream to the leading and trailing edges of the airfoil remained invariant. The four blocks on the upper and lower surface of the airfoil were modified for the specific flap sizes by creating a single block over the flap, while maintaining the overall nodal distribution over the airfoil. This resulted in a change in the number of nodes per block, but a nearly constant ratio of block volume to the number of nodes.

Numerical Method

CMB (Carleton Multi Block) employs a second-order cell-centered finite volume discretization of the Navier-Stokes equations. Discretization of the convective terms employs Osher's scheme, with MUSCL variable interpolation. Central-differencing is used for the diffusive terms. Steady flow

calculations proceed in two parts, initially running an explicit scheme to smooth out the flow solution, then switching to an implicit scheme to obtain faster convergence. The preconditioning is based on block incomplete lower-upper surface factorization and is also decoupled between blocks to increase the parallel performance. The linear system arising at each implicit step is solved using a generalized conjugate gradient method [15]. An implicit unfactored dual-time method is used for the unsteady part of the code. The code is second-order accurate in time. Although a wide range of turbulent models is available in the code, the calculations presented in this paper were achieved with the SST turbulence model. This appears superior in capturing turbulent effects near and far from a solid surface. This is important for modeling dynamic stall, in which crucial elements are boundary layer separation and the convection of the dynamic stall vortex.

The code has been modified to permit the relative motion of surfaces in order to allow for flap actuation.

Verification of the Numerical Method

A grid dependence test was performed by creating a medium and coarse mesh by halving the number of nodes to 41,500 and 21,500, respectively. Figs. 7 and 8 show the comparison of C_l and C_m histories for the three grid levels. While the coarse mesh shows some agreement with the medium mesh, it lacks the resolution necessary to accurately predict the fine details in the lift and pitching moment coefficient histories. The fine mesh and the medium mesh, on the other hand, are closely matched, demonstrating little deviation in lift coefficient, and only minor deviation between the pitching moments. Thus the medium mesh of 41,500 nodes was used for the remainder of the simulations.

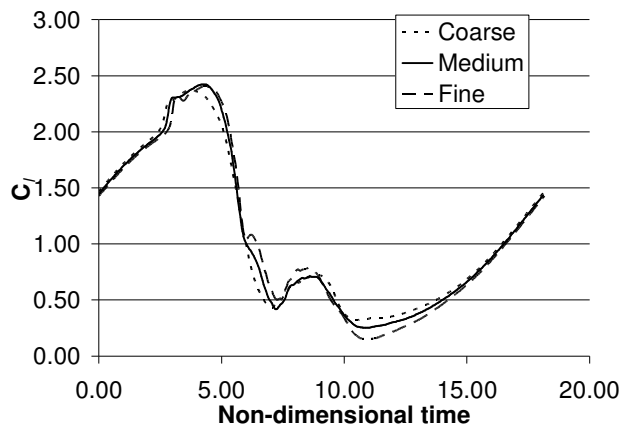


Figure 7: C_l history for the mesh dependency test.

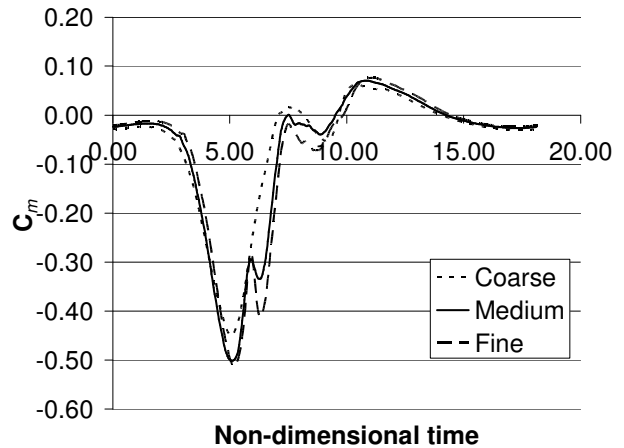


Figure 8: C_m history for the mesh dependency test.

Validation of the Numerical Method

A comparison of the medium mesh results to the experimental data [16] showed good agreement in terms of time histories (Figs. 9 & 10). The magnitude of peak C_l was underpredicted, although the general trend of the curves showed good agreement. The C_m history is in better agreement with the measurements both in terms of the magnitude of minimum C_m and the general trends of the curves. The deviations could likely be due to experimental errors since more extensive validation shows good agreement with other experimental results over a range of Mach and Reynolds numbers and reduced frequencies [10].

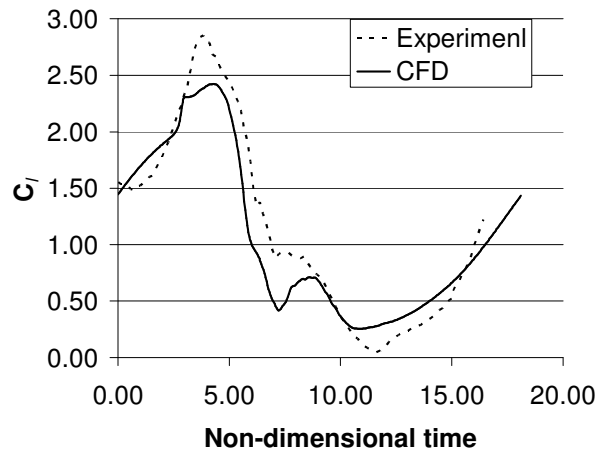


Figure 9: C_l history of CFD validation.

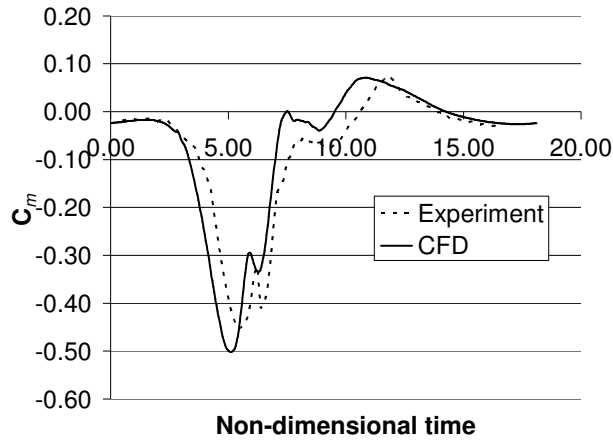


Figure 10: C_m history of CFD validation.

Results

The aim of employing the ACF at high advance ratios is to reduce peak negative pitching moment and negative aerodynamic damping, which is directly associated with stall flutter and vibrations. The torsional damping factor (D.F.) will be calculated as defined by Leishman [17],

$$D.F. = \oint C_m(\alpha) d\alpha. \quad (3)$$

This corresponds to the area inside the C_m - α loop and it can be shown that counterclockwise loops result in positive aerodynamic damping, while clockwise loops result in negative aerodynamic damping. A reduction in negative aerodynamic damping will result in a reduction in vibration and stall flutter.

Parametric Studies

First, a parametric study was performed to determine the optimum flap size and flap deflection. The baseline case for this parametric study was that of a 15% chord flap, with 15° upward deflection. The effect of the flap size was studied by changing the chord length to 10% and 20%, while keeping the baseline deflection of 15°. The effect of the flap deflection was examined by changing the flap deflection to 10° and 20° while keeping the baseline flap size of 15%.

Since the flap cannot alter the formation of the dynamic stall vortex, all flapped cases were run with the same actuation timing. The optimum flap timing appeared to start somewhat after the formation of the dynamic stall vortex, in the 3rd quarter of the azimuth as indicated in Fig. 11. The best duration of

the flap actuation was found to be approximately one quarter of the revolution, i.e. 90° azimuth angle.

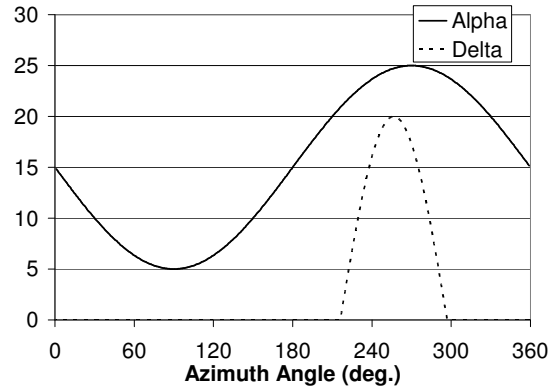


Figure 11: Flap deflection (δ) referenced with α .

The C_r - α and C_m - α loops for the constant flap size study are shown in Figs. 12 and 13, respectively. The C_r - α loop indicates a slight decrease in the dynamic lift when the flap is deflected. The decrease is most pronounced with the largest flap deflection, although the shape of the loop is inherently similar for all three cases. The C_m - α loop indicates that there is a decrease in the peak negative pitching moment, and a corresponding decrease in the size of the second loop, i.e. that of negative aerodynamic damping. Again, the largest decrease occurs with the maximum flap deflection.

The results of the constant deflection study are shown in Figs. 14 and 15. Similar to above, the constant deflection study shows a slight reduction in dynamic lift, and a pronounced reduction in the negative pitching moment and negative aerodynamic damping.

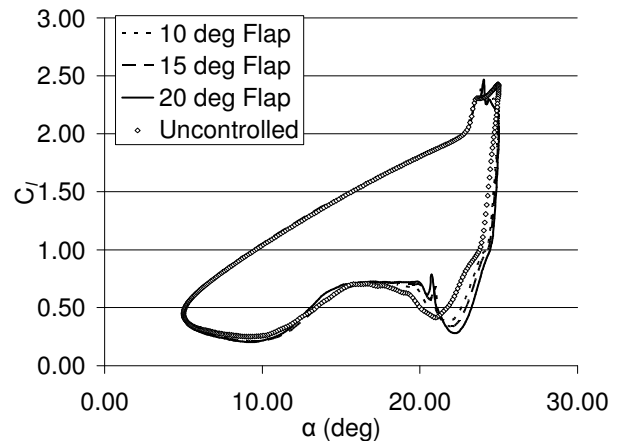


Figure 12: Effect of flap deflection on the C_r - α curve. All cases with 15% chord flap.

The decrease in negative pitching moment corresponds to an increase in flap size. The magnitude of change in negative pitching moment is very small for the constant deflection case, when compared to the changes yielded by the different flap deflections for a constant flap size. However, even small changes in the negative pitching moment result in a measurable reduction of the negative damping loop.

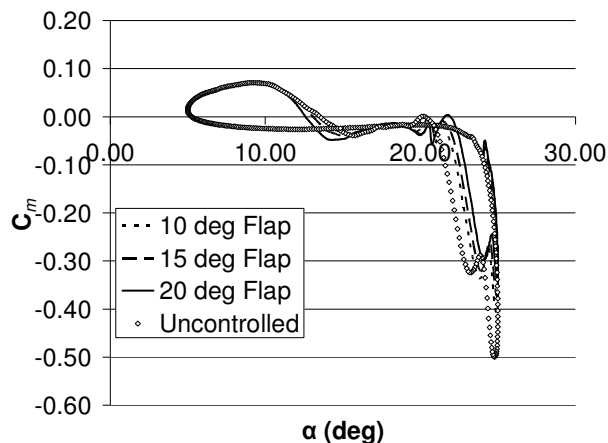


Figure 13: Effect of flap deflection on the C_m - α curve. All cases with 15% chord flap.

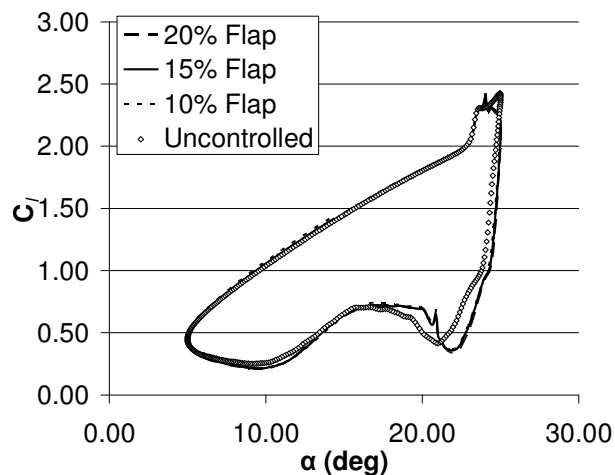


Figure 14: Effect of flap size on the C_r - α curve. All cases with 15° flap deflection.

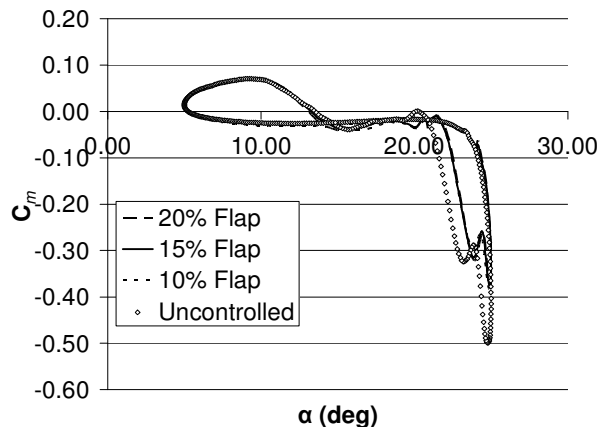


Figure 15: Effect of flap size on the C_m - α curve. All cases with 15° flap deflection.

Optimum Flap Actuation

The maximum reduction in peak negative moment resulted from the use of the 20% chord flap, with a deflection of 20°. This was the most aggressive case. It resulted in a 32% reduction of C_m , and a 54% reduction in negative aerodynamic damping. Interestingly, these reductions come at virtually no dynamic lift penalty, as shown in Figs. 16 and 17. This may be attributed to the fact that dynamic stall is dominated by vortex lift, as opposed to conventional aerodynamic lift. These results correspond to the largest flap size and deflection. This indicates that larger flap sizes and deflections may result in even greater reductions of the pitching moment and negative damping loop, although these might be beyond the limits of practicality in terms of blade structural strength and flap actuation capabilities.

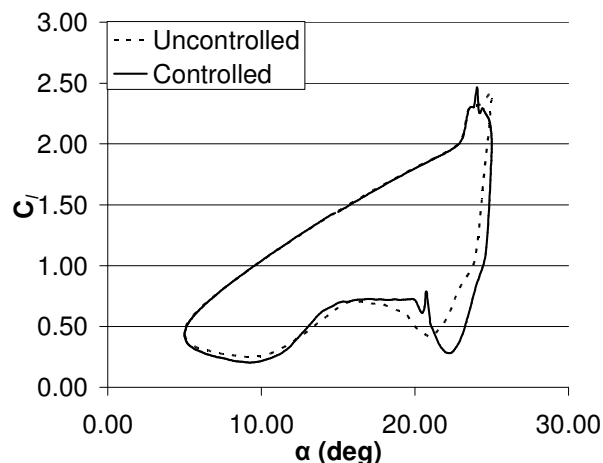


Figure 16: C_r - α curve for most optimum deflection. Flap Chord 20%, flap deflection 20°.

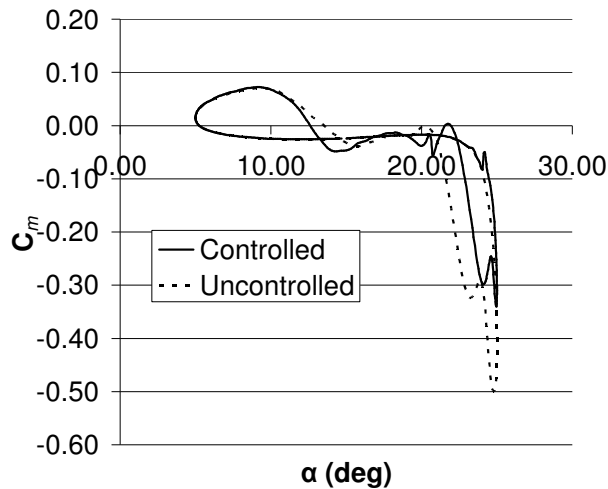


Figure 17: C_m - α curve for most optimum deflection. Flap Chord 20%, flap deflection 20°.

Flow Physics

Flow visualizations were used to examine the effect of the flap on the flowfield, and in particular the mechanism of pitching moment and aerodynamic damping reduction. In both cases, the airfoil encountered leading edge stall, with a dynamic stall vortex convected downstream along the airfoil. As this vortex passed above the trailing edge, a trailing edge vortex was induced. This was true in both the controlled and uncontrolled cases.

The application of the flap seemed to reduce the pressure difference between the upper and lower surfaces of the airfoil. This appears to decrease the peak negative pitching moment. The effect of the flap is indicated on the pressure contour plots shown for $\alpha=23^\circ$ on the downstroke of the cycle, Figs. 18 & 19.

Conclusion

It has been demonstrated using CFD that an actively controlled trailing edge flap has the potential of reducing vibrations due to dynamic stall on helicopter rotor blades. Two different actuation strategies were considered.

For the moderate advance ratio case ($\mu=0.35$) 3D simulations were performed. The 10° upward deflection of the flap resulted in mean amplitude reduction of 23% for the internal structural reactions in the vertical direction. The peak moments corresponding to pitch link loads experienced an average reduction of 44%. These results suggest that the downward deflection of the actively control -

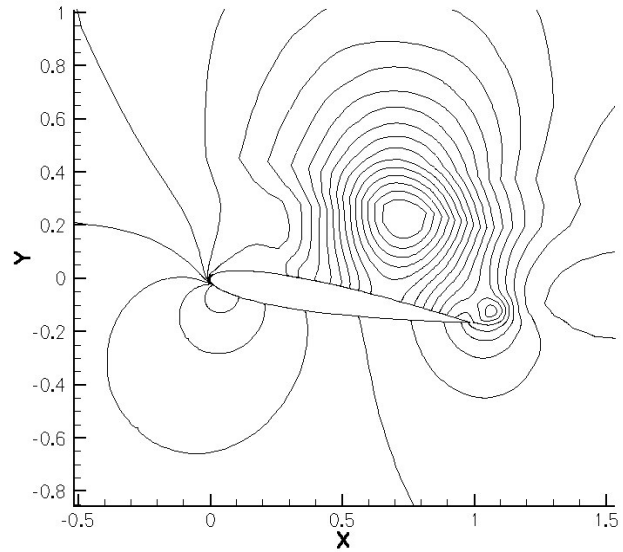


Figure 18: Pressure contours for the uncontrolled case at $\alpha=23^\circ$.

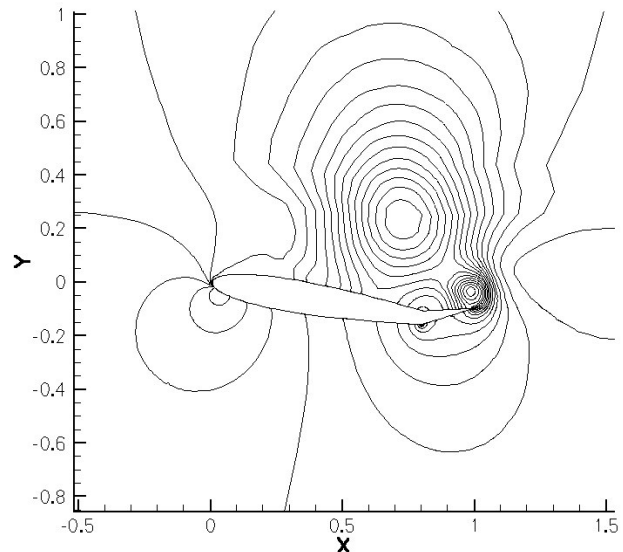


Figure 19: Pressure contours for the controlled case at $\alpha=23^\circ$, $\delta=20^\circ$.

led flap over the retreating portion of the rotor azimuth is an effective means of reducing, or perhaps eliminating, the effects of dynamic stall on the rotor blades.

This test case was specifically tuned to position the rotor in the dynamic stall regime with no flap deflection, and consequently keep the rotor free of the dynamic stall regime when the flap is deflected. This is the suggested use for the downward flap deflection in the retreating portion of the rotor azimuth.

For high advance ratios, 2D simulations were performed to test the rotor blades in deep dynamic stall. The flap deflection was not tuned to correspond to a change in angle of attack, as was the case in the 3D simulations. The 2D study was done with the aim of controlling the strength of the trailing edge vortex to mitigate the effects of dynamic stall.

The flap strategy was to permit the stall to occur as in the clean case, and then deflect the trailing edge flap based upon the location of the convecting dynamic stall vortex. The flap was deflected upwards, which served to reduce the pressure gradient between the upper and lower surfaces of the trailing edge of the airfoil. This resulted in a slight displacement of the dynamic stall vortex, and a considerable change to the resulting negative pitching moment coefficient.

Since C_m is directly related to the damping factor, the reduction in negative C_m resulted in a drop in negative aerodynamic damping, thereby reducing susceptibility to stall flutter and vibration. The most profound reductions occurred in the case of 20° flap deflection with a relative chord length of 20%. In this case, C_m was reduced by 31.9%, resulting in a 54.5% reduction of negative aerodynamic damping.

Based on the reduction of vibration and damping factor for the 3D and 2D cases, the proposed flap actuation presents a preliminary flap actuation strategy. This strategy allows use of the actively controlled trailing edge flap in a broad range of dynamic stall conditions, which improves the desirability of introducing the flap in a production application.

References

[1] Friedmann P.P., Vibration and Noise Reduction Using Actively Controlled Flaps-Their Evolution and Potential for Improving Rotorcraft Technology, *paper no. IF-079, IFASD Conference*, Munich, Germany, 2005.

[2] Kloeppe V., Enekl B. Rotor Blade Control by Active Helicopter Servo Flaps. *Paper no. IF-158 IFASD Conference*, Munich, Germany, 2005.

[3] Depailler G., Friedmann P.P., Alleviation of Dynamic Stall Induced Vibrations Using Actively Controlled Flaps. *American Helicopter Society 58th Annual Forum*, Montreal, Quebec, 2002.

[4] Fulton M.V., Hover Testing of a Small-Scale Rotor with On-Blade Elevons. *AHS Journal, Vol. 46*, April 2001, pp. 96-106

[5] Sekula M., Wilbur M., Yeager W., Aerodynamic Design Study of an Advanced Active Twist Rotor. *AHS International 4th Decennial Specialist's Conference on Aeromechanics, San Fransisco*. 2004, pp. 49-60

[6] Nitzsche F. et al. The SHARCS Project: Smart Hybrid Active Rotor Control System for Noise and Vibration Attenuation of Helicopter Blades, *Paper no. 052, 31st European Rotorcraft Forum*, Florence, Italy. 2005

[7] Barakos G., Badcock K., Gagliardi A., CFD Simulation of Flow Control Devices for Helicopter Rotors, *CEAS/KATnet Conference*, Bremen, Germany, 2005

[8] Nixon M.W., AHS Technical Committee Highlights: Dynamics 2003-2004. *Vertiflite*, Winter 2004, pp. 52-56

[9] Spletstoesser W.R. et al., The HELINOISE Aeroacoustic Rotor Test in the DNW – Test Documentation and Representative Results, DLR-Mitt. 93-09, DLR, Braunschweig, Germany, 1993.

[10] Feszty D., Gillies E.A., Vezza M., Alleviation of Airfoil Dynamic Stall Moments via Trailing Edge Flap Flow Control. *AIAA Journal*, Vol. 42, no.1, pp 17-25, January 2004.

[11] NTUA Internal Report on the GAST code. Aerodynamics Laboratory, Department of Mechanical Engineering, National Technical University of Athens, Greece, 2005

[12] Opoku D.G., Triantos D.G., Nitzsche F., Voustinas S.G., Rotorcraft Aerodynamic and Aeroacoustic Modelling Using Vortex Particle Methods. *23rd ICAS Congress*, Toronto. 2002

[13] Opoku D.G., Nitzsche F., Acoustic Validation of a New Code Using Particle Wake Aerodynamics and Geometrically-Exact Beam Structural Dynamics. *Aeronautical Journal*, Vol 109, 2005, pp. 257-267

[14] Badcock K.J., Richards B.E. and Woodgate M.A., Elements of Computational Fluid Dynamics on Block Structured Grids Using Implicit Solvers.

Progress in Aerospace Sciences, Vol 36, 2000, pp. 351-392

[15] Beaubien R.J., Nitzsche F., Feszty D., Frequency Domain Solution for Transonic Flutter Using Computational Fluid Dynamics. *Paper no. IF-102, IFASD Conference*, Munich, Germany, 2005.

[16] Galbraith R., Gracey M., Gilmour R., Collected Data for Tests on a NACA 0012 Aerofoil. Volume II: Pressure Data from Oscillatory Tests, University of Glasgow, Aero Report 9208, Glasgow, Scotland, UK, Feb. 1992

[17] Leishman J.G., *Principles of Helicopter Aerodynamics*, Cambridge University Press, 2002.